Machine-Learning Framework for Online Probabilistic Rotor Fault Diagnosis via Strain Data under Varying Flight States

Airin Dutta*, Robert Niemiec†, Fotis Kopsaftopoulos‡, and Farhan Gandhi§
Center for Mobility with Vertical Lift (MOVE), Rensselaer Polytechnic Institute, Troy, NY, 12180

A novel machine-learning probabilistic framework for online rotor fault detection, identification, and quantification in multicopters via strain signals is introduced. The framework performs robustly under varying flight states, *i.e.,* forward velocity and gross weight configurations, as well as effectively accounts for the effects of gusts. It employs in-flight time-series strain data obtained from a 2-feet diameter hexacopter flying under external disturbances and uncertainty. The proposed scheme relies on out-of-plane strain measurements at each of the multicopter booms to diagnose, i.e. detect, identify and quantify, rotor faults while distinguishing them from the aircraft response to random gusts. A simple perceptron is shown to be both effective and robust for performing simultaneous online rotor fault detection and identification. Next, linear regression models are used to predict the rotor degradation value with 95% confidence intervals using strain data at the boom on which the faulty rotor is mounted. Indicative results for test operating conditions (not used in the training phase) demonstrate the generalization capability of the method. The proposed framework can accurately detect, identify and quantify minor rotor faults of 10% degradation while distinguishing them from aggressive gusts of up to 10 m/s magnitude. The maximum time of fault detection is less than 0.3 **s while achieving classification and quantification accuracy over 99%.**

Nomenclature

AAM	:	Advanced Air Mobility
FDI	:	Fault Detection and Identification
FP	:	Functionally Pooled
IMU	:	Inertial Measurement Unit
ML	:	Machine Learning

I. Introduction

Advanced air mobility (AAM) powered by autonomous electric VTOL (eVTOL) aircraft is set to revolutionize urban and rural transport by adding a third dimension of mobility. Its capabilities are expected to expand beyond on-demand passenger and cargo mobility, surveillance for public safety, humanitarian aid, infrastructure supervision, remote sensing, etc. A technical report by Uber Elevate states that the operational success will require absolute safety and reliability which can be possible through innovation with large amounts of data from real-world operations after the first generation VTOL aircraft are in production [1]. Therefore, the current interest is towards real-time system-level awareness and safety assurance that will enable transition from “automation" to “autonomy" [2] in AAM vehicles. The goal of this line of work is the development of a data-driven and probabilistic rotor fault diagnosis framework in VTOL aircraft utilizing in-flight data streams which will provide online information about rotor faults; this is also a critical function to trigger control reallocation or vehicle reconfiguration to complete the flight safely. Moreover, continuous monitoring of system faults will decrease downtime for scheduled inspection by enabling Condition Based Maintenance (CBM), thereby havving a significant impact as AAM popularity increases, with the alongside increase in both the number of new passenger and freight aircraft (expected 37000+ by the year 2037 [2]), and trips per vehicle (estimated

*Graduate Research Assistant, Mechanical, Aerospace, and Nuclear Engineering, AIAA Student Member
†Lecturer , Mechanical, Aerospace, and Nuclear Engineering, AIAA Member
‡Assistant Professor of Aerospace Engineering, Mechanical, Aerospace, and Nuclear Engineering, AIAA Senior Member
§Redfern Chair Professor in Aerospace Engineering, MOVE Director, Mechanical, Aerospace, and Nuclear Engineering, AIAA Fellow

usage of 3,000 to 5,000 hours/year [1]).

Multicopters, *i.e.,* rotorcraft with more than four rotors being capable of VTOL and performing agile maneuvers, have attracted interest as a feasible platform for the development of future AAM aircraft concepts. They may offer improved performance stemming from their rotor redundancy and allow for increased design flexibility, ability to integrate distributed electric propulsion, and higher fault robustness and compensation capabilities compared to traditional VTOL/rotorcraft [3–6]. Considering their increasing importance and likely widespread use, accurate and robust fault detection and identification (FDI) are critical in order to ensure the vehicles' overall safety and reliability within complex dynamic environments under uncertainty. However, due to the strong dynamic coupling between rotors, fuselage, booms, and control inputs, as well as time-varying, cyclo-stationary, and non-linear behavior, they face certain system modeling and FDI challenges that are not present in fixed-wing aircraft. These issues, as well as potential solutions, have been addressed by (i) various model representations (linear time-invariant, linear parameter varying, and non-linear models) [7–10], (ii) signal processing techniques (in time- and frequency-domain, Kalman filter) [11–16], and (iii) computational intelligence approaches (neural networks, fuzzy logic, hidden Markov models, dynamic Bayesian network, and Gaussian mixture models, support vector machines) [17–25] – for a detailed review please refer to [26]. However, the available studies are either limited by analytical model building with the assumption that the physical knowledge of the system is available, use of arbitrary thresholds for detecting faults, or mostly concentrate on structural faults of blades, propellers, powertrain, etc. in rotorcraft.

The problem of multicopter rotor fault diagnosis under constantly varying operating and environmental conditions is approached via the use of statistical time series methods by the present authors. Such data-driven methods have been mainly used in structural health monitoring [27–30] and for the diagnosis of various types of faults in fixed-wing aircraft systems [31, 32] due to their simplicity, efficient handling of uncertainties, no requirement of physics-based models, and applicability to different operating conditions. Zhao *et al.* have validated a stochastic hybrid system for health evaluation in multicopters under simulated sensor anomalies [33]. In a recent work by the authors, Dutta *et al.* achieved fast and accurate online rotor failure detection and identification via a novel application of stochastic time-series models and proper statistical decision-making under pre-determined confidence levels for a hexacopter flying forward under different turbulence levels and uncertainty as well as varying forward velocity and gross weight [34, 35].

Another class of data-driven methods lies within the machine learning (ML) family of techniques, adept in clustering, classifying, and extracting useful features from high-dimensional and potentially noisy data. Neural networks (NN) [17–19] and support vector machines [24, 25] are widely used in FDI to make a decision on the current state of a dynamic system. Ganguli *et al.* [18] and Morel *et al.* [17] employed NNs to detect and trace faults and defects of helicopter rotor blades using noise-contaminated vibration data. Multicopter rotor structural damage detection and identification has been demonstrated by Iannace *et al.* in Ref. 19 with acoustic signals and NNs, and by Bondrya *et al.* in Ref. 25 via support vector machines based on measurements of acceleration from the onboard IMU (Inertial Measurement Unit). To address issues related to lack of physical insight and explainability with ML algorithms, Dutta *et al.* proposed a time-series assisted neural network for online rotor FDI [36]. The features, acting as the input layer of the NN, were extracted from a statistical time-series model of the healthy aircraft for improved physical explainability of the data-driven scheme. .

To the authors' best of knowledge, papers pertaining to actuator fault quantification in rotorcraft are scarce. Fault magnitude information obtained online can facilitate the transition to optimal/robust control scheme and planning alternative trajectories with limited control authority depending on the fault severity. In an attempt to fill this research gap, the time-series assisted neural network which was previously developed by Dutta *et al.* was extended to determine three discrete fault levels (mild, caution, and urgent) in addition to rotor fault detection and classification while differentiating them from random gusts [37]. To enable continuous fault quantification, a unified statistical time-series framework was developed based on Functionally Pooled (FP) models that are capable of representing aircraft dynamics under rotor faults for a continuum of fault magnitudes of a particular rotor fault type [38]. This framework was applied to a flexible-boom hexacopter using remote signals from the Inertial Measurement Unit (IMU) and local signals from sensors placed on individual booms. Besides accurate fault detection and identification with either type of signal, improvement in continuous rotor fault quantification was observed for local signals over remote (IMU) signals.

The objective of this paper is the introduction and assessment of a novel data-driven, computationally efficient, framework for online rotor fault detection, identification, and quantification in multicopters operating under multiple flight states and external disturbances. Data collected from local strain sensors mounted on the multicopter booms are used to enable probabilistic model learning that triggers the fault diagnosis stage. The performance of the developed framework with respect to fast rotor fault detection, accurate identification, gust distinction capability, and precise quantification under turbulence, random gusts, and rotor faults is investigated with a substantial amount of test data sets.

II. Hexacopter Model and Data Generation

A. Physics-Based Modeling of Multicopter System

A flight simulation model has been developed for a regular hexacopter (Fig. 1) using the summation of forces and moments to calculate aircraft accelerations. This model is used as the source of simulated data under varying operating and environmental conditions, as well as different fault types. Rotor loads are calculated using Blade Element Theory coupled with a 3×4 Peters-He finite-state dynamic wake model [39]. This model allows for the simulation of abrupt rotor failure by ignoring the failed rotor inflow states and setting the output rotor forces and moments to zero. A feedback controller is implemented on the nonlinear model to stabilize the aircraft altitude and attitudes, as well as track desired trajectories written in terms of the aircraft velocities. This controller is designed at multiple trim points, with gain scheduling between these points to improve performance throughout the flight envelope. The control architecture is detailed in Ref. 40. This control design has been demonstrated to perform well even in the event of rotor 1, 2, or 6 failure, with no adaptation in the control laws themselves. The 12 rigid body states are defined as:

$$\mathbf{x} = \begin{Bmatrix} X & Y & Z & \phi & \theta & \psi & u & v & w & p & q & r \end{Bmatrix}^T \tag{1}$$

The input vector is comprised of the first four independent multirotor controls for collective, roll, pitch and yaw and is defined in Eq. 2:

$$\mathbf{u} = \begin{Bmatrix} \Omega_0 & \Omega_R & \Omega_P & \Omega_Y \end{Bmatrix}^T \tag{2}$$

The booms of the hexacopter are modeled as one-dimensional Euler-Bernoulli beams with an added tip mass and loading, and are coupled to the rigid body motion of the vehicle. The positive bending deflections in the in-plane and out-of-plane of the hub are illustrated in Fig. 2. Torsion and axial deformation are neglected. The beam equations are discretized in space using the Ritz method with 2 modes in direction, as given in Eq. 3), with polynomial shape functions, ϕ that satisfy the geometric boundary conditions given by Eq. 4. To facilitate the inversion of the mass matrix that arises from this discretization, these polynomials are chosen to be orthogonal. The modes are obtained via eigen-analysis of the beam in a vacuum.

$$v = \sum_{i=1}^{2} \eta_{v_i}(t)\phi_{v_i}(l) \qquad w = \sum_{i=1}^{2} \eta_{w_i}(t)\phi_{w_i}(l) \tag{3}$$

where, η represents the modal deformations. l is the non-dimensional boom coordinate, representing the distance of a point on the boom from its root normalized by the boom length. It ranges from 0 to 1, denoting the boom root and boom tip, respectively. The geometric boundary conditions are given by*:

$$w(0) = w'(0) = 0 \qquad v(0) = v'(0) = 0 \tag{4}$$

*The symbols ' ' ' and ' ' ' designate $\frac{d}{dl}$ and $\frac{d}{dt}$, respectively.

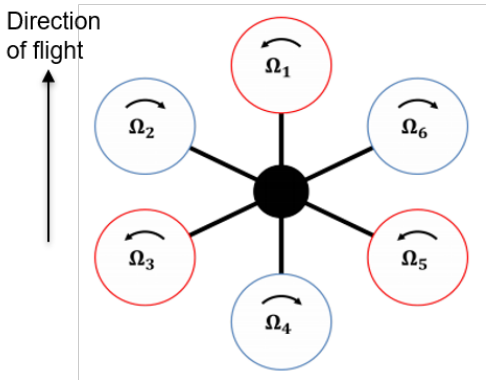

Fig. 1 Hexacopter schematic

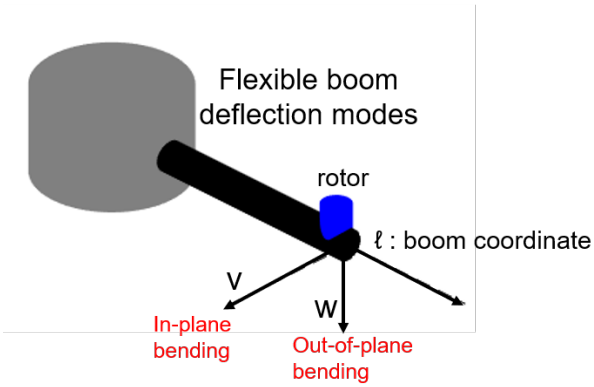

Fig. 2 Flexible boom deformation

The eight states for each flexible boom are defined as follows:

$$\mathbf{x} = \left\{ \eta_{w_1} \quad \eta_{w_2} \quad \eta_{v_1} \quad \eta_{v_2} \quad \dot{\eta}_{w_1} \quad \dot{\eta}_{w_2} \quad \dot{\eta}_{v_1} \quad \dot{\eta}_{v_2} \right\}^T \tag{5}$$

The sensor signals can be calculated using the above aircraft states obtained from the flight simulation (Appendix A).

B. Incorporation of Turbulence

A continuous Dryden wind turbulence model [41] has been incorporated in the flight simulation model to replicate realistic flight conditions. The Dryden model is dependent on altitude, length scale, direction-cosine matrix, body velocity, and turbulence intensity. It outputs the linear and angular velocity components of continuous turbulence as spatially varying stochastic signals. These signals are added to the inflow of each of the rotors by transforming them from the aircraft center-of-gravity to the corresponding rotor locations, to account for the effect of the turbulent wind velocities on the multicopter. The proper combination of the turbulence block parameters determines the fit of the signals to observed turbulence [42]. In this system, the altitude is taken as 5 m, and the length scale as the hub-to-hub distance of the hexacopter which is 0.6096 m (2 ft). The direction-cosine-matrix and forward velocity are determined from the instantaneous aircraft states during the simulation.

C. Introduction of Gusts

Next, data sets under different magnitude (5 m/s to 10 m/s) and directions of gusts for healthy flight under severe turbulence have been generated [43]. The gusts follow a '1-cosine' shape with a gradual increase, followed by a steady-state and gradual decrease [44], as shown in Fig. 3a. In the simulations, the gusts commence at 2 s with a gradual increase from 0 to its full magnitude in the next 2 s, after which it becomes steady and lasts for 2 s, before gradually decreasing to zero again in the next 2 s. Therefore, in the simulated data gusts last from 2-8 s in a span of 10 s of healthy flight. In real flight, the magnitude, direction, commencement time, and duration of gusts can be random in nature depending upon the region, altitude, and weather conditions. The wind velocity directions are denoted by unit vectors with the positive X, Y, Z directions shown in Fig. 3b.

D. Data Generation

The data sets are generated through a series of simulations for various operating conditions ranging from a forward speed of 4 m/s to 8 m/s and a gross weight of 2 to 4 kg. For gust-affected healthy flights, gusts of different magnitudes, *i.e.,* 5, 8.67, and 10 m/s, and various directions are considered. The rotor fault types addressed in this paper are front rotor (rotor 1), right-side rotor (rotor 2), and left-side rotor (rotor 6) faults (See Fig. 1). Rotor degradation of different magnitudes has been replicated by reducing the commanded speed of that particular rotor with a multiplier ranging from 0 to 1, where '0' denotes 0% rotor degradation, *i.e.,* healthy aircraft and '1' implies 100% rotor degradation or

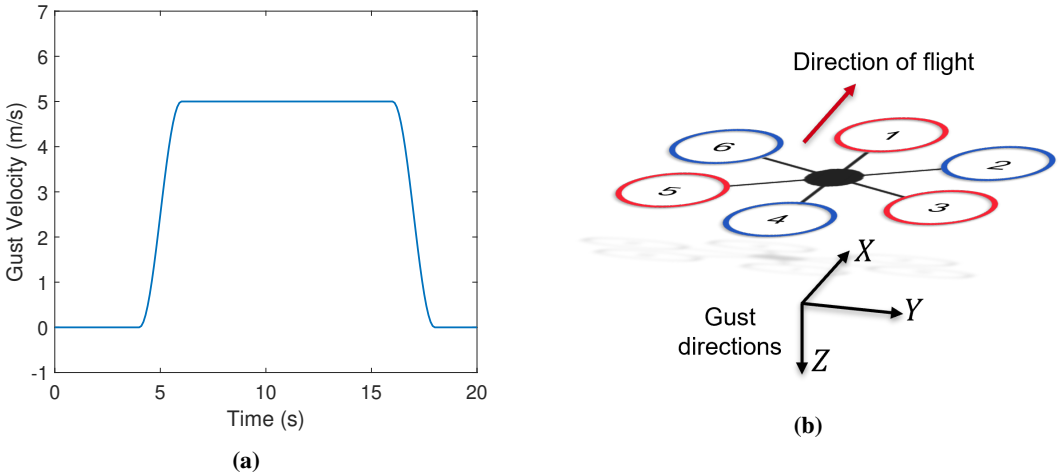

Fig. 4 Indicative gust profile: (a) magnitude of gusts with time and (b) direction of gust.

Table 1 Summary of generated data sets

Phase	Health conditions	Operating states	Rotor fault levels / Gust magnitudes / Turbulence levels	Signal Length
Training Data	Healthy flight	(4,5,6,7,8) m/s × (2,3,4) kg	Severe turbulence	50 s
	Gust affected healthy flight	(4,6,8) m/s × (2,4) kg	8.67 m/s and 8 directions	10 s
	Rotor 1,2, and 6 faults	(4,5,6,7,8) m/s × (2,3,4) kg	10, 50, 90 % degradation	50 s
Testing Data	Healthy flight	(4.5,5.5,6.5,7.5) m/s × (2.5,3.5) kg	Severe turbulence	30 s
		(4,5,6,7,8) m/s × (2,3,4) kg	Light turbulence	30 s
	Gust affected healthy flight	(4.5,5.5,6.5,7.5) m/s × (2.5,3.5) kg	5 m/s and 6 directions 10 m/s and 6 directions	10 s
	Rotor 1, 2, and 6 faults	(4,5,6,7,8) m/s × (2,3,4) kg	20, 30, 40, 60, 70, 80, 100 % degradation	50 s
		(4.5,5.5,6.5,7.5) m/s × (2.5,3.5) kg	20, 40, 60, 80, 100 % degradation	30 s

Sampling frequency: $F_s = 10$ Hz

complete rotor failure. The data sets generated under different operating and health conditions considered in this paper are summarized in Table. 1. From here onward, "modeled" flight states or rotor degradation levels mean that the training data sets were generated under these operating conditions, and the rest of the operating conditions are referred to as "unmodeled".

III. Methodology

In a previous study, a sensor signals based statistical time series method, capable of effective fault detection, identification, and magnitude estimation within a unified framework for a hexacopter flying under turbulence and uncertainty was presented [38]. The method is based on the functionally pooled (FP) models (whose parameters are functions of the operating conditions), and proper statistical decision-making schemes. FP models are capable of accurately representing the aircraft dynamics under rotor faults for a continuum of fault magnitudes of a particular rotor fault type. These models for different rotor faults on a multicopter can be identified from available time-series sensor data in the baseline phase. In its inspection phase, there are three distinct steps taking place within a probabilistic framework: step I involves fault detection, step II involves fault identification after rotor fault compensation by the controller, and step III involves precise fault quantification within the identified type of fault. Fault magnitude is continuous, involving an infinite number of potential fault magnitudes ranging from healthy to complete failure. The validity and effectiveness of the method have been assessed via a proof-of-concept application to rotor fault diagnosis with remote and local signals, i.e., z-acceleration signal from the system IMU and the z-accelerations at the respective boom-tips, respectively. It has been demonstrated that effective fault detection, fault mode identification, and fault magnitude estimation with uncertainty bounds is possible even for "unmodeled" (not used in training) rotor degradation with a very limited number of sensor signals (even with a single response signal from the IMU) through powerful signal analysis techniques. An important observation was that fault quantification performance, i.e., the accuracy of fault estimation and tightness of uncertainty bounds were improved via the use of local sensors (boom accelerations) compared to remote sensors (body acceleration).

However, when gusts are introduced in healthy flight, the above method falsely detects the response of the healthy

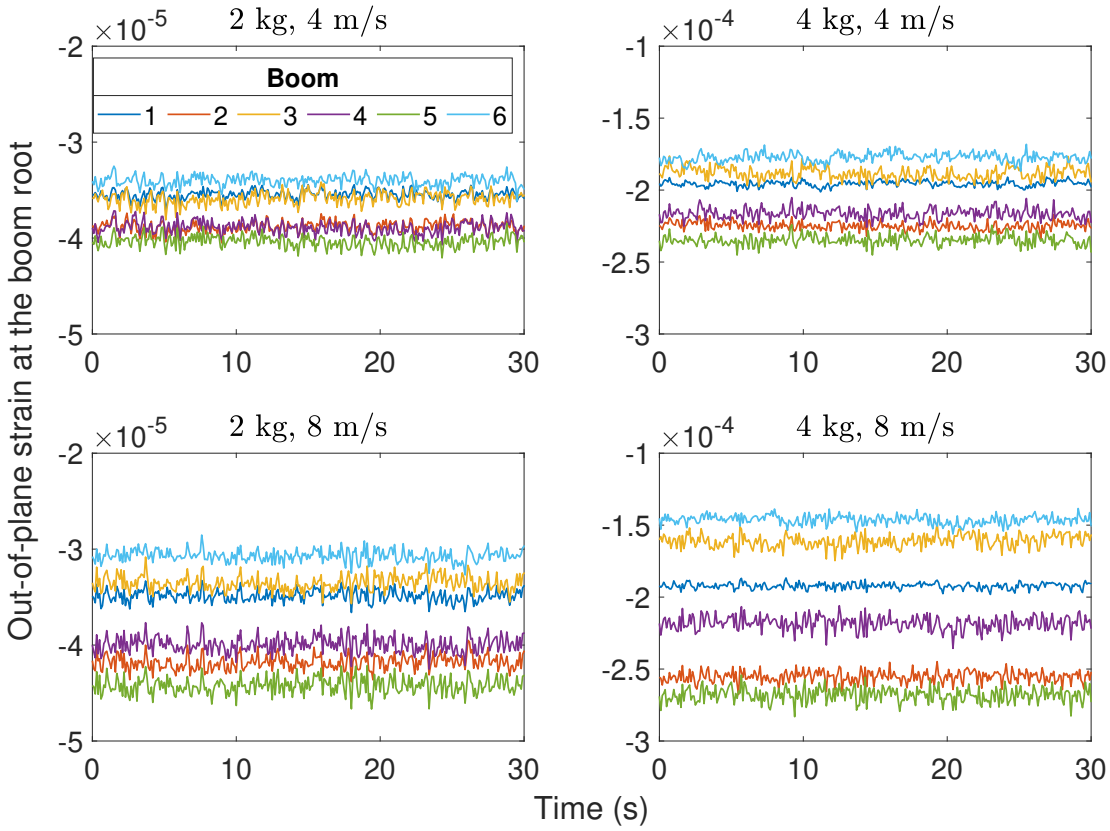

Fig. 5 Healthy flight strain signals under various forward speed and gross weight configurations (the actual configuration is indicated above each subplot).

aircraft to gusts as rotor faults, with both the remote and the local signals. To account for random gusts the method needs to be significantly extended, such as identifying several time-varying models with the non-stationary signals under gusts of different wind velocities and directions. Moreover, since these methods involve the identification of dynamic models from signals, the signals need to be sampled at a relatively higher rate after proper filtering to capture the aircraft dynamics and flexible boom natural frequencies. These limitations have motivated the need for other signals which can be extracted from the available instrumentation and contain more information regarding rotor faults.

A. Sensor Signals and Indicative Data

Strain gauges are common sensors that are bonded directly onto aerospace structures to measure stresses along load-bearing components. Nowadays, they are finding increasing applications in "smart" civil structures for continuous health monitoring. Future AAM vehicles are most likely to be equipped with strain gauges on all the booms for early detection of structural faults, cracks, and defects. Hence, with these available sensors, individual rotor speeds can be monitored from the respective strain gauge readings, since the magnitude of the strain on each of the booms will depend on the thrust produced by the rotor mounted on it. Actual rotor speeds can give physical insight into the controller commands under rotor faults, and random gusts. In practice, the sensor readings will be stochastic in nature due to sensor noise, and external disturbances during the flight. Therefore, the rotor fault diagnosis framework should be able to account for the noise and uncertainty in the signals. It should be noted that this rotor diagnosis framework is based on these available in-flight sensor signals only.

Flight simulation for the hexacopter was performed at operating conditions specified in Table 1. Figures 5 through 8 show signal time histories of strain gauges placed at all the boom roots (where the boom connects to the hub) for cases of healthy flight with and without gusts, and different rotor fault scenarios under different operating conditions. The x-axis shows the time in seconds, as the y-axis gives the value of out-of-plane (perpendicular to the rotor hub plane) strain at each of the 6 booms. These local signals, sampled at 10 Hz, will be utilized for the development of

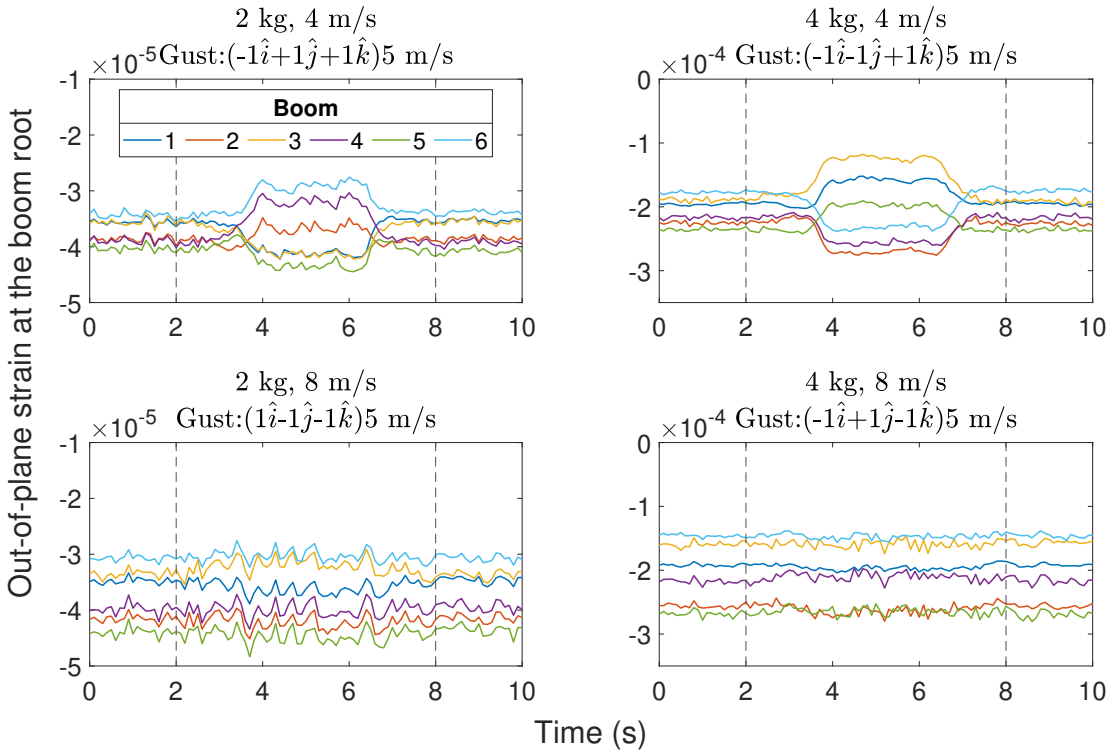

Fig. 6 Indicative healthy flight strain signals under 8.67 m/s gusts from various directions under different operating conditions (indicated above each subplot).

the machine-learning based framework of probabilistic rotor fault detection, identification, and quantification for their certain characteristics, as discussed in the following paragraphs.

Figure 5 show the strain at each of the boom roots in the out-of-plane directions while flying at 4 flight states ((4,8) m/s × (2,4) kg) under severe turbulence in healthy condition. Though the signals are stochastic in nature, they possess a definite statistical mean value for each of the boom. These mean values of the strain on each boom depend on the corresponding rotor thrust and hence the rotor speeds. Thus, these signals give an insight into the commanded rotor speeds, when there are no rotor faults in the system. Note, that due to the coordinate system convention, the strains are expressed in negative values and the lesser values represent more amount of boom strains and consequently higher rotor speeds. Also, the total strain and consequently total rotor thrust is dictated by the gross weight of the aircraft, whereas the differential thrust, reflected in the range of the boom strains depend upon the commanded forward speed under healthy flight.

Figure 6 show the time history of the strain signals under a few indicative gusts of 8.67 m/s considered in this study. The gusts commence at 2 s and last until 8 s, shown by the black dashed vertical lines. There are no rotor faults in the system. In each of the subplots of Fig. 6, the flight states are different and the gusts are coming from various directions (shown in the titles of the subplots). It is evident that there is a significant change in the mean values of strain signals, mostly during the steady gust phase lasting from 4 s to 6 s. It can be observed in the top-left plot that the absolute value of strains in booms 4 and 6 decreases during gust, mimicking a rotor fault, where the rotor loses thrust. The aim of this study is to prevent such situations from being misclassified as rotor faults by considering the response of all the rotors represented by the corresponding strain values at the boom roots.

Figures 7 and 8 shown the strain signals under rotor 1, and 2 faults and their varying magnitudes under a single indicative flight states. For the simulation results presented, the rotor faults occur at $t = 2$ s, as indicated by the vertical black dashed line. It should be noted that due to faults, the signals have a transient response before reaching the controller-compensated steady state. In Fig.7, degradation of rotor 1 has resulted in the decrease of the absolute value of strain on boom 1 due to loss of thrust. To compensate for the yaw imbalance due to this fault, rotor 4 also slows down. Similarly, in Fig.8, the response of other rotors to a rotor 2 fault is seen. Finally, it can be observed that the rotor fault magnitude has a direct relation with the change from the healthy value of strain on the boom it is mounted upon. Under

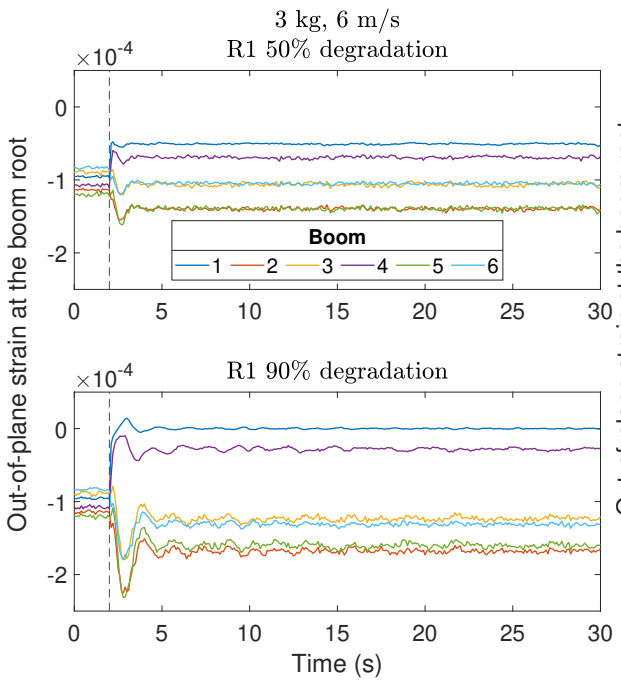

Fig. 7 Indicative out-of-plane strain signals at each boom root under 50% (top) and 90% (bottom) degradation of rotor 1 at 6 m/s and 3 kg.

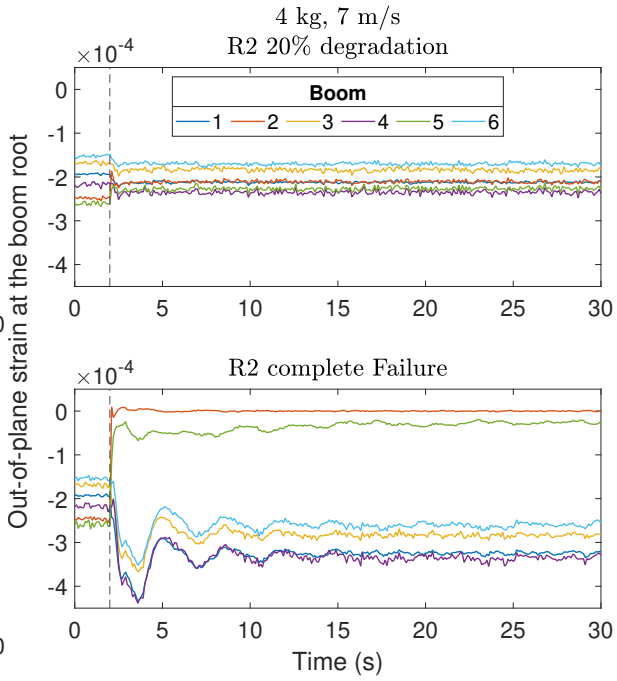

Fig. 8 Indicative of out-of-plane strain signals at each boom root under 20 % (top) and 100 % (bottom) degradation of rotor 2 at 7 m/s and 4 kg.

complete failure of rotors or 100% degradation, the strain value goes to zero, due to zero thrust generated. The variation of strain on the respective boom can be employed to estimate the fault magnitude after it is detected and identified.

The pattern of how the rotors respond to gusts and faults will be utilized to distinguish them. Also, observe that contrary to faults, the change in signals due to gusts lasts only for its duration. Rotor faults cannot be reversed and hence the change in the signals continue through the entire flight time.

B. The Machine-Learning Framework

In this section, the development of a data-driven framework for probabilistic rotor fault diagnosis utilizing the carefully selected in-flight data streams via the application of common ML algorithms is presented. It has been observed from the 6 local signals (out-of-plane strain at all boom roots) that the change in their absolute magnitude closely reflects the actual rotor speeds. Under different operating conditions, such as healthy flight with or without gusts, and different rotor fault scenarios, the statistical mean of signals will change relative to each other, forming some distinguishing patterns. These patterns can be classified via a pattern recognition algorithm, such as a simple perceptron to simultaneously detect and identify faults. If and when a fault is detected, the strain signal from the faulty rotor boom will be used for fault quantification by a simple linear regression framework since the absolute value of strain depends on the rotor speed and consequently the value of degradation. However, a simple normalization of the faulty rotor boom strain will be performed to account for the multiple flight states without any knowledge of the current operating conditions in the inspection phase. The workflow of the proposed rotor FDI technique is given in Fig. 9.

1. Perceptron

Perceptron is a computer learning method devised to simulate the ability of the brain to recognize and discriminate. It is the building block of complex neural networks. This machine learning method enables distributed information processing with neurons arranged in layers and executed in parallel. The neurons are non-linear information processing elements and the interconnections between these neurons are known as weights. These weights are learned through supervised training algorithms, where the training data contain the inputs and their corresponding output labels. Neural

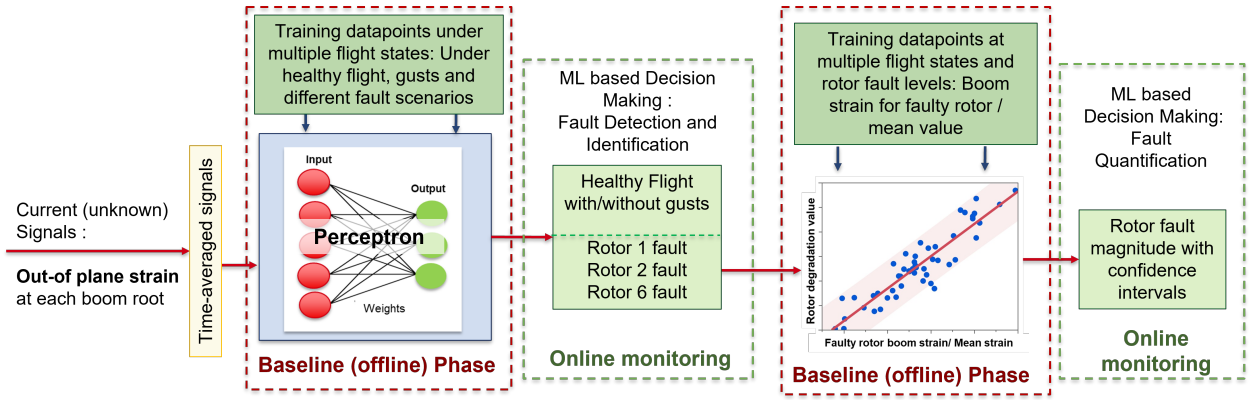

Fig. 9 The proposed machine learning framework for online probabilistic rotor fault detection, identification, and quantification.

networks can compactly represent information, perform excellent classification, and can accommodate noise and uncertainty in data with carefully chosen features and regularization parameters. These characteristics make it attractive for the present application, where the aim is to develop a robust rotor FDI framework with signals affected by atmospheric disturbances encountered in actual flight. But often deep neural networks focus on fitting the data and suffer from a lack of explainability due to a "black-box" model. Moreover, to enable real-time decision-making with limited computational capabilities of the onboard flight computer, a simple perceptron will be employed.

From the previous section, it has been observed that the values of out-of-plane strains at each boom root relative to each other can be a useful feature for a pattern recognition algorithm to determine the aircraft health status. However, to determine the different fault classes from the physical knowledge of the distinctive change in the strain at the boom of the faulty rotor and their diametrically opposite pair will require nested decision-making trees [36]. To this end, a simple perceptron is trained to output one of the 4 linearly separable classes: healthy aircraft, rotor 1 faults, rotor 2 faults, and rotor 6 faults with the mean value of the 6 strain signals over some time window as input. The input layer is denoted by $\boldsymbol{x}^T$ and the output layer is denoted by $\boldsymbol{h}(\boldsymbol{x})$ and is related by the following equation:

$$\boldsymbol{h}(\boldsymbol{x}) = \sigma\left(\boldsymbol{W}^T\boldsymbol{x} + \boldsymbol{B}\right) \tag{6}$$

where, $\sigma(z)$ indicates the softmax activation function[†]. The weight matrix and the bias vector for the layer are denoted by $\boldsymbol{W}$ and $\boldsymbol{B}$ are determined in the baseline training phase by backpropagation learning techniques to minimize classification error. Using the cross-entropy error as cost function and softmax function in the output layer, the probabilities of each input element belonging to a output class can be obtained [45].

The first class is trained with healthy signals under severe turbulence with and without gusts (8.67 m/s with different directions). The rotor 1, 2, and 6 fault classes have been trained with the respective rotor fault signals under 10, 50, and 90% degradation (denoted as training data in Table 1). The training data sets are divided into disjoint windows of 1 s. Each data point consists of the mean of the 6 strain signals that are calculated over the above-mentioned window and its corresponding true class label. The number of data points should be balanced for the different classes to avoid classifier bias. The details of this perceptron are given in Table 2.

2. Linear Regression Model

Assuming that the mean of the out-of-plane strain at the faulty rotor boom varies linearly with the rotor fault magnitude, a linear regression model is fitted (MATLAB function: *fitlm.m*) as follows:

$$y = \boldsymbol{x}\boldsymbol{\beta} + \epsilon \qquad \boldsymbol{x} = [1 \quad x] \qquad \boldsymbol{\beta} = [\beta_1 \quad \beta_2]^T \tag{7}$$

[†]Softmax activation function, $\sigma(z_j) = \dfrac{e^{z_j}}{\sum_{i=1}^{C} e^{z_i}}$, C: no. of output classes, $\boldsymbol{z} = \left(\boldsymbol{W}^T\boldsymbol{x} + \boldsymbol{B}\right)$

Table 2 Details of the perceptron training

Specifications	Value
Input Type	Out-of-plane strain at all boom roots
Input Layer Size	6
Training Function	Levenberg-Marquardt optimization
Hidden Layer Size	**0**
Output Classes	4 (Healthy and Rotor 1,2, & 6 faults)
Cost Function	Cross-Entropy
Activation Function	Softmax
Data Partition	Learning: Validation: Test = 50:25:25 % of Training Data
Performance	1.3×10^{-3}

where 'y' denotes the rotor degradation value, 'x' normalized strain at faulty rotor boom and '$\boldsymbol{\beta}$' the vector of coefficients to be learnt from the training data. The normalized strain, 'x' is calculated as following:

$$x = \frac{\mu_\varepsilon - \varepsilon_{\text{faulty rotor boom}}}{\mu_\varepsilon} \qquad \mu_\varepsilon = \frac{1}{6}\sum_{i=1}^{6} \varepsilon_i \tag{8}$$

where, ε_i represents the strain at 'i'th boom root, and μ_ε denotes the mean value of all the strains. Note, that the total rotor speed, and consequently the mean of all the strain values are maintained at the same value before and after the rotor fault initiation, to support the weight of the aircraft. The normalization of strain is required for taking into account the change in rotor strains with the various forward speeds and gross weights. Faulty rotor strain for the same rotor degradation will be different for different flight states. This step helps map the value of faulty rotor boom strain linearly with the rotor degradation, such that the normalized value is 1 for complete rotor failure under all flight states.

The linear regression models are trained with the faulty training data denoted in Table 1. For rotor 1 faults, the strain on boom 1 normalized with the mean of all 6 strains is used, with the labels being the true rotor degradation values. Similarly, for rotor 2, and 6 faults, the normalized strain signals from boom 2 and 6 are used for training, respectively. The respective fault models output the predicted rotor fault magnitude, once the fault is identified along with the 95% confidence intervals according to Scheffé's method. The details of the trained linear regression models are given in Table 3.

IV. Results and Discussion

Current in-flight data streams have been used for online monitoring of the aircraft health condition. A window of 1 s of each of the 6 signals has been processed through workflow depicted in Fig. 10. To ensure continuous decision-making, the window is updated every 0.1 s. The computation time required to make a decision is less than 0.01 s, which is less than the window update time, making it suitable for real-time monitoring. A fault is detected when the perceptron outputs any class other than healthy, and that output class determines which of rotors 1,2, or 6 has failed, enabling simultaneous fault detection and identification. Note that this decision is attached with a probability estimate which

Table 3 Details of the linear regression models

Specifications	Value
Inputs	Out-of-plane strain at faulty rotor boom divided by the mean strain of all the booms
Number of coefficients	2
R^2 fit	0.98, 0.97, 0.97 for rotor 1, 2, and 6 fault models, respectively
RMSE	3.73, 5.72, 5.49 % rotor degradation for rotor 1, 2, and 6 fault models, respectively
Output	Rotor degradation with confidence intervals

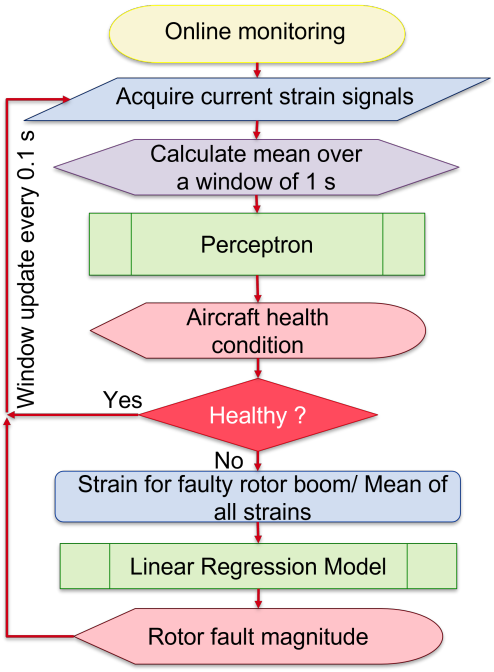

Fig. 10 Flowchart for online monitoring of rotor faults via the proposed framework.

can help the operator to have a better insight of the fringe cases such as confusion between very mild degradation and strong gusts where the probability estimates of the two confusing classes will be about 50%, whereas in normal cases the confidence of a decision is generally more than 95%. After fault detection and identification, the linear regression model predicts the fault magnitude and its 95% confidence intervals using the normalized strain from the boom on which the faulty rotor is mounted.

A. Indicative Results for Online Health Monitoring

Few indicative results for online monitoring of aircraft health with the current decision-making framework have been presented in Figs. 11a through 13b. The top subplots show the mean of signals over a window of 1 s , updated every 0.1 s, that are used as input to the decision-making framework. The bottom subplots show the decision output by the framework, at each time window. The x-axis shows the time of flight in seconds in both plots. Since it is required to collect signals for the required time window initially the online monitoring starts at 1 s. If the decision marker is shown in +, the aircraft is healthy. Otherwise, the markers *, o, and x denote fault of rotor 1,2, and 6 respectively. The fault magnitude is shown by the y-axis in the bottom plots.

Figure 11a shows the correct health prediction for a healthy flight under light turbulence. It can be observed that the decision marker remains green (+), denoting healthy flight even under operating conditions of 5.5 m/s and 2.5 kg, a flight state not used during the training phase.

Figures 11b and 12a, demonstrates accurate health monitoring even under aggressive gusts of magnitude 10 m/s and 8.67 m/s, respectively and unmodeled flight states. The aircraft responds to maintain its commanded speed under such gusts, causing significant changes in the aircraft dynamics (See Appendix B, Figs.15 and 16). Moreover, in Fig. 12a it can be clearly seen that the absolute value of strain for boom 1 decreases to counter the gust, thus mimicking a rotor 1 fault. But with the trained perceptron based on local signals, the health of the aircraft encountering both of these indicative gusts are correctly classified as a healthy aircraft.

Figures 12b to 13b, show indicative results for online monitoring under rotor faults. Note that for the results presented both the operating conditions and the rotor fault magnitudes (80, 60, and 20% degradation) considered were not used in the training phase. In the top plots, the time of fault commencement is shown in black vertical dashed lines. In the bottom plots, the time of fault detection is shown in brown vertical dashed lines. In the bottom plots the true value of rotor degradation is shown by a grey horizontal line. The fault detection and classification, is depicted by the marker colour changing from green (+) to red, blue, or violet (*/ o / x) depending on the rotor fault. If the true fault magnitude lies within the 95% confidence intervals of the predicted values (shown by the vertical segments at

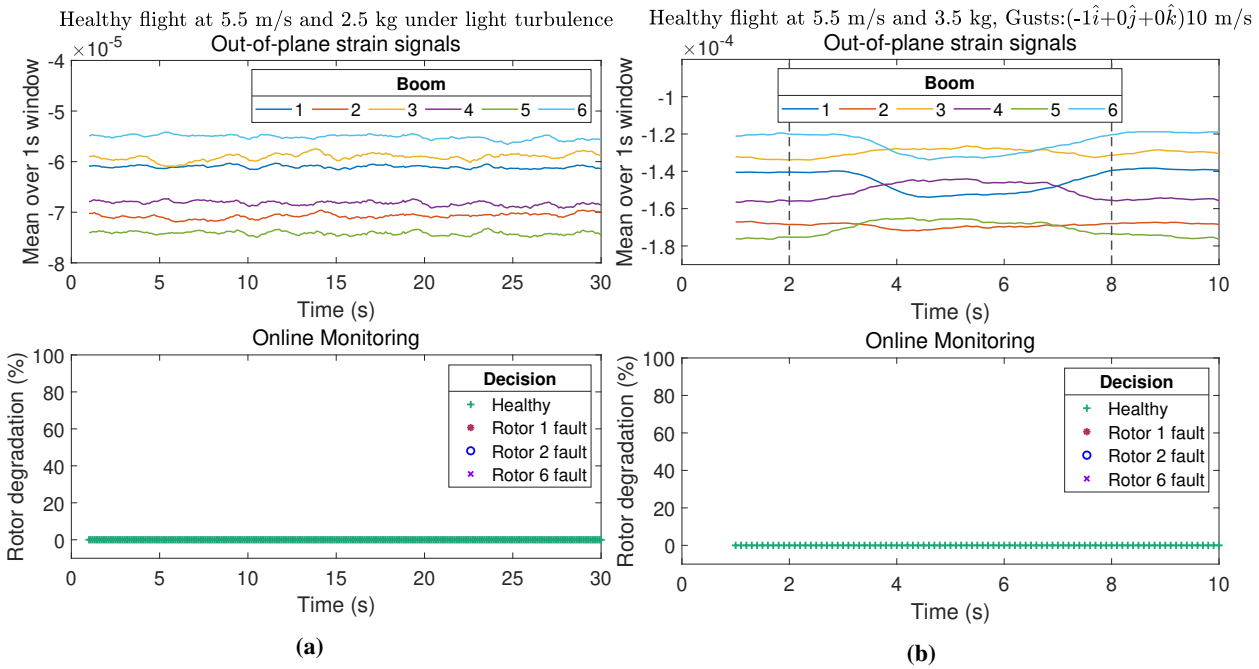

Fig. 11 Indicative diagnostic results during the online inspection phase: (a) healthy flight under light turbulence, and (b) healthy flight with gust of 10$(-1\hat{i}+0\hat{j}+0\hat{k})$ m/s.

each decision marker), it denotes a correct fault quantification. The precision of fault quantification, i.e., the absolute difference between the predicted and true value, is represented by the proximity of the predicted values and the true value of rotor degradation.

Figure 12b shows correct rotor fault diagnosis of rotor 1 80% degradation. The fault is detected and classified within 0.1 s of the commencement, denoted by the green marker changing to red in the bottom plot. However, just after the fault detection and classification, depicted by the marker colour changing from green, the fault quantification becomes accurate only after the transient phase of the signals are over and they become steady (as shown in the top plots). This is also due to the fact that the signals are time-averaged over 1 s. Thus, the fault is accurately quantified within 1 s of the fault commencement, evident by the true rotor degradation lying in between the 95% confidence intervals shown in red error bars. Also, it can be observed that fault quantification is quite precise since the true value and the predicted values are very close to each other. Similar speed of rotor FDI, and efficiency of quantification is observed for rotor 2, and 6 faults in Figs.13a and 13b, respectively. It is evident that a fault is always detected within 0.3 s of its commencement with a longer time needed for mild degradation levels, as is seen in Fig.13b, where a 20% rotor fault needs 0.3 s to be detected.

B. Summary Results

The change in the mean values of out-of-plane signals under different rotor faults can be analyzed with logical AND and OR functions, to detect and classify them. Hence, the perceptron is capable of efficient rotor FDI even under various unknown operating conditions which have not been used to train it. This property, known as the generalization capability of the perceptron has been demonstrated with the test data in the inspection phase. The flight conditions include intermediate forward speeds and gross weights, light levels of turbulence in healthy flight, gusts of higher magnitudes, and unmodeled rotor fault levels (for details, see Table 1). The performance of this framework on test data is summarized in Tables 4a and 4b. For each dataset, a number of decisions are made throughout the flight time with moving windows. The fault classification and quantification accuracy denote the percentage of those decisions where the correct health condition is determined, and whether the true rotor degradation value lies in between the predicted 95% confidence intervals, respectively. The fault prediction error gives the error in point estimation of the fault magnitude, and its' mean, and standard deviation are given in rotor degradation magnitude (% rotor degradation).

It is observed that though the perceptron was trained with healthy data under certain flight states and severe turbulence

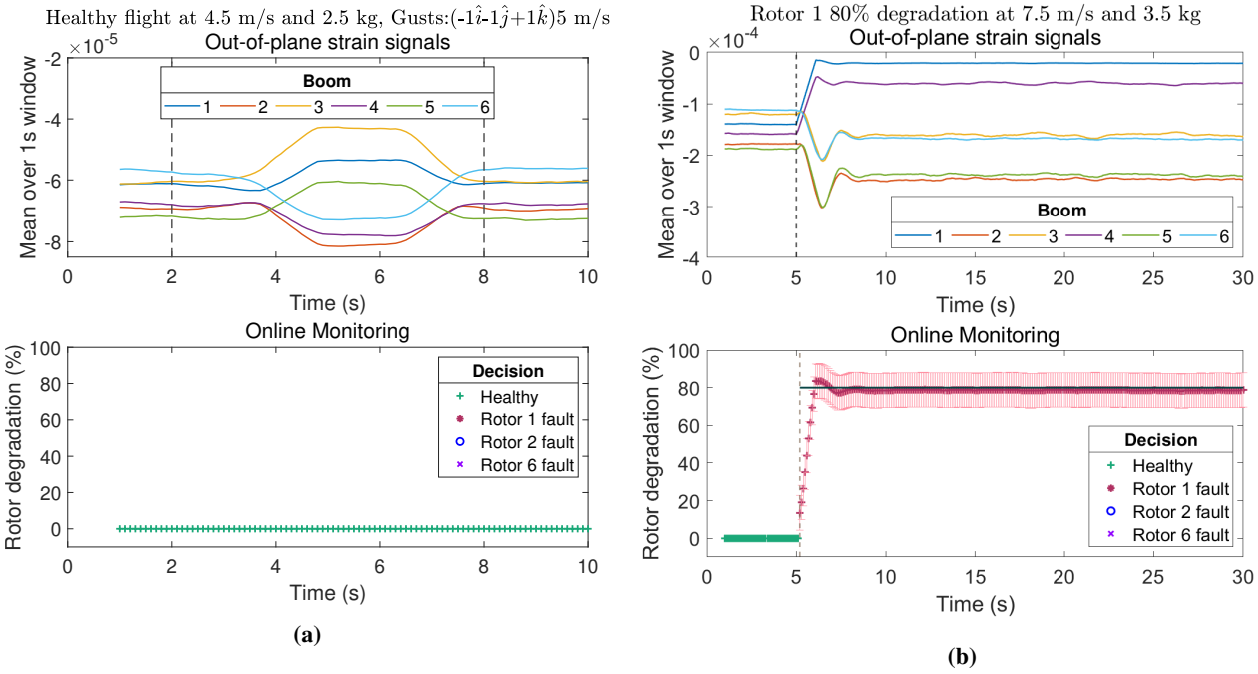

Fig. 12 Indicative diagnostic results during the online inspection phase: (a) healthy flight with gust of 5$(-1\hat{i}-1\hat{j}+1\hat{k})$ m/s, and (b) 80 % degradation of rotor 1.

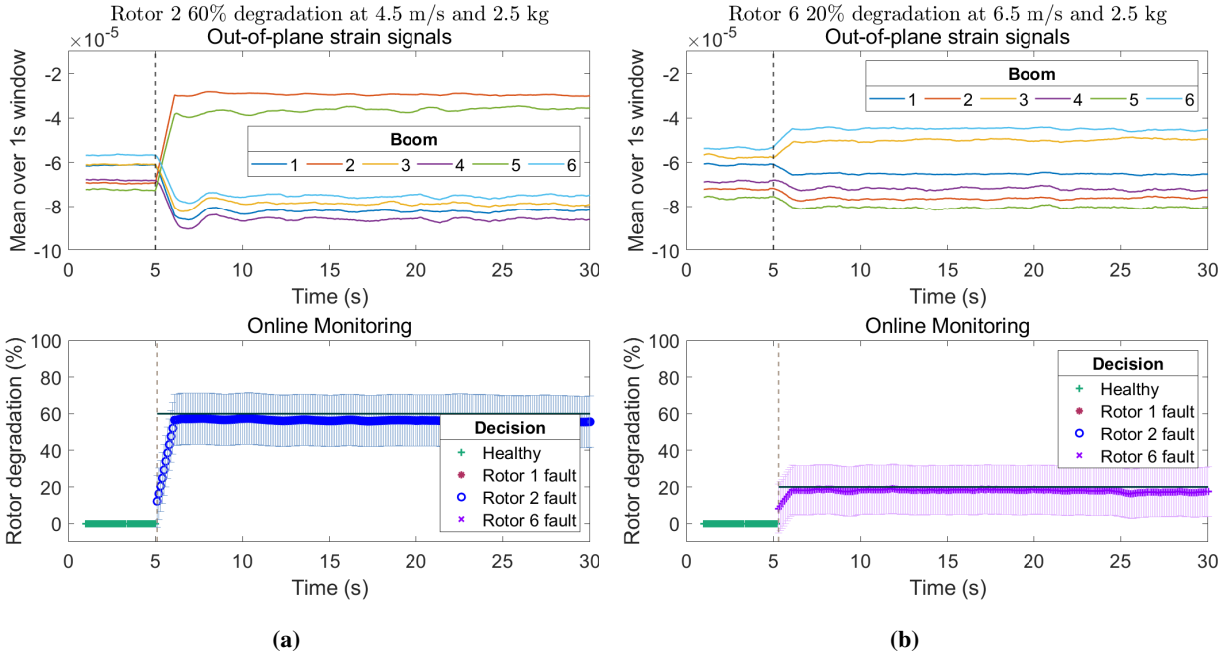

Fig. 13 Indicative diagnostic results during the online inspection phase: (a) 60 % degradation of rotor 2, and (b) 20 % degradation of rotor 6.

only, it gives perfect classification with intermediate flight states, and light turbulence levels too (See Table 4a).

For gusts, even with unmodeled flight states, gust directions, and gust magnitudes (higher and lower than used for training the perceptron), the health condition classification accuracy is maintained over 99%.

Table 4 Summary results for rotor fault detection, identification, and quantification

(a) Healthy aircraft under turbulence and gusts

Health condition	Operating condition	Classification accuracy (%)
Healthy flight	Unmodeled flight states & severe turbulence	100
	Modeled flight states & light turbulence	100
Healthy flight under gusts	Unmodeled flight states & 5 m/s gusts	99.3
	Unmodeled flight states & 10 m/s gusts	99.6

(b) Faulty aircraft

Operating condition	Health condition	Classification accuracy (%)	Quantification accuracy (%)	Fault Prediction error (% degradation)		Average time of fault detection (s)
				Average Value	Standard Deviation	
Modeled fight states & unmodeled degradations	Rotor 1 faults	100	99.1	4.34	2.39	0.280
	Rotor 2 faults	100	99.1	5.14	3.45	0.198
	Rotor 6 faults	99.9	99.3	4.18	4.29	0.236
Unmodeled fight states & unmodeled degradations	Rotor 1 faults	100	99.1	4.58	2.55	0.237
	Rotor 2 faults	100	99.2	5.50	2.97	0.152
	Rotor 6 faults	99.9	99.2	4.34	3.83	0.190

The rotor faults under both modeled and unmodeled operating conditions, as well as intermediate degradation levels which have not been considered in the training phase, have been classified accurately (See Table 4b). The fault quantification accuracy is over 99%. Here, the slight decrease in the accuracy can be attributed to the fact that in the transient phase of the signals the fault magnitude is incorrectly predicted as lesser than the correct value that is obtained with steady signals. The fault prediction error i.e., the difference between the predicted and true value of fault magnitude, averaged over all datasets and decision points is 4.7 % rotor degradation. The standard deviation of the fault prediction error is about 3.2 % rotor degradation. Lower values the mean and standard deviation of the fault prediction error implies that the fault quantification will be accurate with tight confidence intervals. The average and maximum of the range of 95% confidence intervals is 18 % and 28% rotor degradation, respectively. The fault detection time will be in multiples of the window update interval, i.e. 0.1 s. The maximum time to detect a fault is 0.3 s. Mild rotor faults require more time to be detected, and faults over 50% degradation generally require 0.1 s. The average time of fault detection is calculated by averaging over all the test data sets and it is observed to be less than 0.3 s.

V. Conclusions

This paper introduced a novel probabilistic ML framework for online rotor fault detection, identification (classification), and quantification. The assessment of the method was presented for a 2-feet diameter (rotor hub-to-hub distance) hexacopter operating at various forward speeds and gross weights under turbulence, gusts, and uncertainty. In the baseline phase, simple and computationally efficient ML algorithms, *i.e.,* a perceptron and linear regression model, are trained on the basis of out-of-plane strain signals measured from strain gauges placed at each one of the boom roots. In the inspection phase, there are two distinct steps taking place within a probabilistic framework: step I involves simultaneous rotor fault detection and identification and step II involves fault quantification within the identified type of fault. Fault magnitude is considered to be continuous, involving an infinite number of potential fault magnitudes ranging from healthy to complete failure. The effectiveness of the method has been assessed via application to a number of "unmodeled" aircraft operating as well as health conditions. The method is well-suited for online health monitoring of multicopters as demonstrated by the speed of decision-making under any admissible operating condition, excellent accuracy with regard to distinguishing gusts from rotor faults, and precise fault magnitude estimation with corresponding

uncertainty bounds.

The main conclusions drawn from this study are summarized as follows:

- The study – including the proof-of-concept application – has demonstrated that effective fault detection, fault type identification, and fault magnitude estimation are possible based on judiciously selected signals from the onboard sensor network.
- The embedded information pertaining to the aircraft rotors' health condition under multiple flight states can be extracted from boom strain signals via simple and computationally light ML algorithms such as perceptron and linear regression models.
- Robust and accurate rotor fault detection, identification, and quantification for a hexacopter under various forward speed and gross weight configurations have been achieved in real-time under different levels of turbulence, random gusts, and uncertainty.
- Simultaneous rotor fault detection and identification occurs almost immediately after the fault commencement, even for mild rotor degradation.
- Fault magnitude estimation is excellent, both at the nominal (point estimation) level and at the probabilistic level with close uncertainty bounds.
- The ML framework is better suited for real-time monitoring of aircraft health than the nominal unified statistical framework without any significant augmentation provided proper signals from the instrumentation to monitor the strain on individual booms are used.

Acknowledgments

This work was supported by the U.S. Air Force Office of Scientific Research (AFOSR) grant "Formal Verification of Stochastic State Awareness for Dynamic Data-Driven Intelligent Aerospace Systems" (FA9550-19-1-0054) and Program Officer Dr. Erik Blasch.

Appendix

A. Sensor Signals

The data used in this study are obtained from simulation rather than experiments and therefore the sensor signals need to be calculated from the available aircraft states.

Generally, Inertial Measurement Units (IMUs) are composed of a 3-axis accelerometer and a 3-axis gyroscope and outputs the body accelerations (x, y, and z acceleration) and the angular rates (roll, pitch, pitch and yaw rates), which can be determined from 12 rigid body states are defined in Eq. 1 as follows:

$$\begin{aligned} \text{Body accelerations} &= \begin{bmatrix} \dot{u} & \dot{v} & \dot{w} \end{bmatrix}^T \\ \text{Angular rates, } \omega &= \begin{bmatrix} p & q & r \end{bmatrix}^T \end{aligned} \tag{9}$$

These signals are referred to as remote signals.

The sensors mounted on the different locations on the individual booms, such as strain gauges and accelerometers are referred to as the local signals. These can be computed from the individual booms modal deformation states and shape functions (Eqs. 5 and 3) using the following expressions:

$$\begin{aligned} \text{Total deformation, } q &= \begin{cases} \sum_{i=1}^{2} \phi_{w_i}(l)\eta_{w_i} & \text{Out-of-plane} \\ \sum_{i=1}^{2} \phi_{v_i}(l)\eta_{v_i} & \text{In-plane} \end{cases} \\ \text{Strain, } \epsilon &= \begin{cases} \sum_{i=1}^{2} \phi''_{w_i}(l)\eta_{w_i} \times a/2 & \text{Out-of-plane} \\ \sum_{i=1}^{2} \phi''_{v_i}(l)\eta_{v_i} \times b/2 & \text{In-plane} \end{cases} \end{aligned} \tag{10}$$

where, a and b are the width and height of the cross-section of the boom, respectively. l is the distance from the boom root where the sensor has been placed, normalized by the boom length.

The accelerometer readings on each of the boom can be calculated as:

$$\text{Acceleration} = \ddot{r} = \omega \times \dot{r} + \dot{\omega} \times r + \omega \times \omega \times r \tag{11}$$

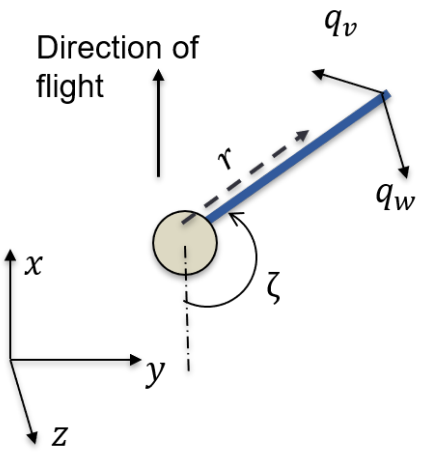

Fig. 14 Position of a boom with respect to the hub and its deformations.

Table 5 Boom properties

Parameters	Value
Boom Length (L)	0.2617 m
Material	Aluminium
Cross-section	Hollow square
Outer dimension	0.0156 m
Inner dimension	0.0130 m
Flexural Rigidity	179 Nm^2

where,

Distance of accelerometer from the hub,

$$r = \begin{bmatrix} -L\cos\zeta \\ L\sin\zeta \\ -d \end{bmatrix} + \begin{bmatrix} -\sum_{i=1}^{2} \phi_{v_i}(l)\eta_{v_i}\sin\zeta \\ -\sum_{i=1}^{2} \phi_{v_i}(l)\eta_{v_i}\cos\zeta \\ \sum_{i=1}^{2} \phi_{w_i}(l)\ddot{\eta}_{w_i} \end{bmatrix}$$

Here, ζ is the azimuth angle of the boom (See Fig. 14), L is the length of the boom and d is the vertical position of the boom from the center-of-gravity of the aircraft. The boom properties are given in Table 5.

Note that these derivations are shown for a single time instant, t. Repeating this computations for the entire range of time will generate the time-series sensor data.

B. Aircraft Response to Gusts

Figure 15 shows the pitch response of the hexacopter to a 10 m/s gust coming directly from the direction of flight, which effectively increases the flight speed. This is countered by the controller by decreasing the nose-down pitch to maintain flight at the commanded speed of 5.5 m/s. To that end, the speed of rotor 1 increases, and that of rotor 4 decreases, indicated by the change in the mean value of strain evident in Fig. 11b. Similarly, a gust of magnitude 8.67 m/s and having a sideways component, causes the aircraft to roll significantly while the gust lasts, when compared to a healthy flight without gusts, as shown in Fig. 16.

References

[1] "Fast-Forwarding to a Future of On-Demand Urban Air Transportation," Tech. rep., October 2016.

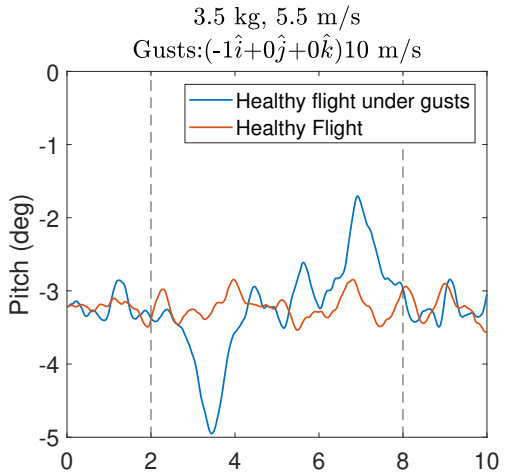

Fig. 15 Change in longitudinal dynamics in response to gusts.

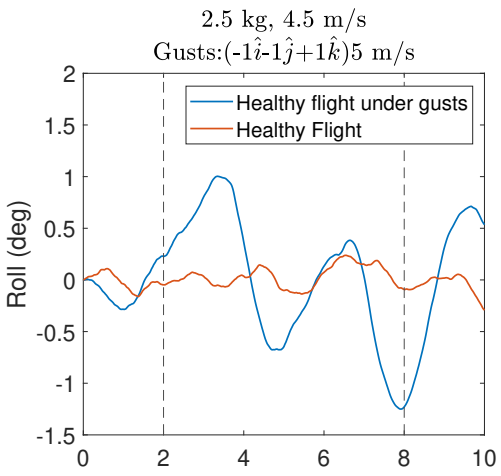

Fig. 16 Change in lateral dynamics in response to gusts.

[2] "Automation vs. Autonomy in Urban Air Mobility," , November 2019. URL `https://www.airbus.com/newsroom/stories/automation-autonomy-in-urban-air-mobility.html`, [Online; accessed 3-September-2020].

[3] McKay, M. E., Niemiec, R., and Gandhi, F., "Analysis of Classical and Alternate Hexacopter Configurations with Single Rotor Failure," *Journal of Aircraft*, Vol. 55, No. 6, 2018, pp. 2372–2379. https://doi.org/10.2514/1.C035005.

[4] Frangenberg, M., Stephan, J., and Fichter, W., "Fast Actuator Fault Detection and Reconfiguration for Multicopters," *AIAA Guidance, Navigation, and Control Conference, Kissimmee, Florida*, 2015. https://doi.org/10.2514/6.2015-1766.

[5] Kim, K., Rahili, S., Shi, X., Chung, S.-J., and Gharib, M., "Controllability and Design of Unmanned Multirotor Aircraft Robust to Rotor Failure," *AIAA Scitech 2019 Forum, San Diego, CA*, 2019. https://doi.org/10.2514/6.2019-1787.

[6] Raabe, C. T., "Adaptive, Failure-Tolerant Control for Hexacopters," *AIAA Infotech@Aerospace (I@A) Conference, Boston, MA*, 2013.

[7] "System Identification Modeling of a Small-Scale Unmanned Rotorcraft for Flight Control Design," Vol. 47, No. 1, 2002, pp. 50–63. https://doi.org//10.4050/JAHS.47.50.

[8] Freddi, A., Longhi, S., Monteriù, A., and Prist, M., "Actuator Fault Detection and Isolation System for an Hexacopter," *IEEE/ASME 10th International Conference on Mechatronic and Embedded Systems and Applications*, IEEE/ASME, 2014. https://doi.org/10.1109/MESA.2014.6935563.

[9] D. Hyunchul Shim, H. J. K., and Sastry, S., "Control system design for rotorcraft-based unmanned aerial vehicles using time-domain system identification," *IEEE International Conference on Control Applications, Anchorage, AK*, IEEE, 2000. https://doi.org/10.1109/CCA.2000.897539.

[10] Navarro, P., Cho, S., Rashid, A., Ruiz, A., and Bhandari, S., "Flight Testing, Data Collection, and System Identification of a Multicopter UAV," *AIAA Modeling and Simulation Technologies Conference, Grapevine, TX*, AIAA, 2017. https://doi.org/10.2514/6.2017-1558.

[11] Waschburger, R., Paiva, H. M., e Silva, J. J. R., and Galvão, R. K. H., "Fault detection in a laboratory helicopter employing a wavelet-based analytical redundancy approach," *Conference on Control and Fault-Tolerant Systems, Nice, France*, 2010, pp. 70–75.

[12] Schwartz, B. C., and Jones, D. L., "Quadratic and instantaneous frequency analysis of helicopter gearbox faults," *Mechanical Systems and Signal Processing*, Vol. 14, No. 4, 2000, pp. 579–595.

[13] Williams, W. J., and Zalubas, E. J., "Helicopter transmission fault detection via time-frequency, scale and spectral methods," *Mechanical Systems and Signal Processing*, Vol. 14, No. 4, 2000, pp. 545–559.

[14] Gopalratnam, G., Zorn, C., and Koch, A., "Multisensor Data Fusion for Sensor Failure Detection and Health Monitoring," *AIAA Guidance, Navigation, and Control Conference and Exhibit, San Francisco, CA*, 2005.

[15] Cox, J. R., Arnold, S., and Anusonti-Inthra, P., "Rotor Blade Fault Detection through Statistical Analysis of Stationary Component Vibration," *52nd AIAA/SAE/ASEE Joint Propulsion Conference*, 2016. https://doi.org/10.2514/6.2016-4642.

[16] Lu, F., Li, Z., Huang, J., and Jia, M., "Hybrid State Estimation for Aircraft Engine Anomaly Detection and Fault Accommodation," *AIAA Journal*, Vol. 58, No. 4, 2020, pp. 1748–1762. https://doi.org/10.2514/1.J059044.

[17] Morel, H., Ouladsine, M., Krysinski, T., and Brun-Picard, D., "Defect detection and tracing on helicopter rotors by artificial neural networks," *IEEE Advanced Process Control Applications for Industry Workshop, Vancouver, Canada*, 2005.

[18] Ganguli, R., Chopra, I., and Haas, D. J., "Helicopter Rotor System Fault Detection Using Physics-Based Model and Neural Networks," *AIAA Journa*, Vol. 36, No. 6, 1998, pp. 1078–1086.

[19] Gino Iannace, G. C., and Trematerra, A., "Fault Diagnosis for UAV Blades Using Artificial Neural Network," *Robotics*, Vol. 8, No. 3, 2019. https://doi.org/10.3390/robotics8030059.

[20] Ganguli, R., "Health Monitoring of a Helicopter Rotor in Forward Flight Using Fuzzy Logic," *AIAA Journal*, Vol. 40, No. 12, 2002.

[21] Chen, Z., and Yang, Y., "Fault diagnostics of helicopter gearboxes based on multi-sensor mixtured hidden markov models," *ASME Journal of Vibration and Acoustics*, Vol. 134, No. 3, 2012.

[22] Wang Min, H. N.-q., and Guo-jun, Q., "A method for rule extraction based on granular computing: Application in the fault diagnosis of a helicopter transmission system," *Journal of Intelligent and Robotic Systems*, Vol. 71, 2013, pp. 445–455.

[23] Ochoa, C. A., and Atkins, E. M., "Multicopter Failure Diagnosis through Supervised Learning and Statistical Trajectory Prediction," *2018 AIAA Information Systems-AIAA Infotech @ Aerospace, Kissimmee, Florida*, 2018. https://doi.org/10.2514/6.2018-1636.

[24] Baskaya, E., Bronz, M., and Delahaye, D., "Fault detection diagnosis for small UAVs via machine learning," *2017 IEEE/AIAA 36th Digital Avionics Systems Conference (DASC)*, 2017, pp. 1–6.

[25] Bondyra, A., Gąsior, P., Gardecki, S., and Kasiński, A., "Fault diagnosis and condition monitoring of UAV rotor using signal processing," 2017, pp. 233–238. https://doi.org/10.23919/SPA.2017.8166870.

[26] Qi, X., Theillol, D., Qi, J., Zhang, Y., and Han, J., "A Literature Review on Fault Diagnosis Methods for Manned and Unmanned Helicopters," *International Conference on Unmanned Aircraft Systems*, 2013.

[27] Fassois, S., and Kopsaftopoulos, F., *New Trends in Structural Health Monitoring*, Springer, 2013, Chap. Statistical Time Series Methods for Vibration Based Structural Health Monitoring, pp. 209–264. https://doi.org/10.1007/978-3-7091-1390-5.

[28] Kopsaftopoulos, F. P., and Fassois, S. D., "Scalar and Vector Time Series Methods for Vibration Based Damage Diagnosis in a Scale Aircraft Skeleton Structure ," *Journal of Theoretical and Applied Mechanics*, Vol. 49, No. 4, 2011.

[29] Samara, P. A., Fouskitakis, G. N., Sakellariou, J. S., and Fassois, S. D., "A Statistical Method for the Detection of Sensor Abrupt Faults in Aircraft Control Systems," *IEEE Transactions on Control Systems Technology*, Vol. 16, No. 4, 2008, pp. 789–798. https://doi.org/10.1109/TCST.2007.903109.

[30] Kopsaftopoulos, F. P., and Fassois, S. D., "A vibration model residual-based sequential probability ratio test framework for structural health monitoring," *Structural Health Monitoring*, Vol. 14, No. 4, 2015, pp. 359–381.

[31] Dimogianopoulos, D. G., Hios, J. D., and Fassois, S. D., "FDI for Aircraft Systems Using Stochastic Pooled-NARMAX Representations: Design and Assessment," *IEEE Transactions on Control Systems Technology*, Vol. 17, No. 6, 2009, pp. 1385–1397.

[32] Dimogianopoulos, D., Hios, J., and Fassois, S., "Aircraft engine health management via stochastic modelling of flight data interrelations," *Aerospace Science and Technology*, Vol. 16, No. 1, 2012, pp. 70–81. https://doi.org/10.1016/j.ast.2011.03.002.

[33] Zhao, Z., Quan, Q., and Cai, K.-Y., "A Health Evaluation Method of Multicopters Modeled by Stochastic Hybrid System," *Aerospace Science and Technology*, Vol. 68, 2017, pp. 149–162. https://doi.org/10.1016/j.ast.2017.05.011.

[34] Dutta, A., McKay, M., Kopsaftopoulos, F., and Gandhi, F., "Statistical residual-based time series methods for multicopter fault detection and identification," *Aerospace Science and Technology*, Vol. 112, 2021, p. 106649. https://doi.org/https://doi.org/10.1016/j.ast.2021.106649, URL https://www.sciencedirect.com/science/article/pii/S1270963821001590.

[35] Dutta, A., McKay, M., Kopsaftopoulos, F., and Gandhi, F., "Rotor Fault Detection and Identification on a Hexacopter under Varying Flight States Based on Global Stochastic Models," *Vertical Flight Society 76th Annual Forum, Online (due to COVID-19)*, AHS, 2020.

[36] Dutta, A., McKay, M., Kopsaftopoulos, F., and Gandhi, F., "Fault Detection and Identification for Multirotor Aircraft by Data-Driven and Statistical Learning Methods," *Electric Aircraft Technologies Symposium (EATS), Indianapolis, IN*, AIAA/EATS, 2019.

[37] Dutta, A., McKay, M., Kopsaftopoulos, F., and Gandhi, F., "Rotor Fault Detection and Identification for a Hexacopter Based on Control and State Signals via Statistical Learning Methods," *Vertical Flight Society 76th Annual Forum, Online (due to COVID-19)*, AHS, 2020.

[38] Dutta, A., Niemiec, R., Kopsaftopoulos, F., and Gandhi, F., "Unified Statistical Framework for Rotor Fault Diagnosis on a Hexacopter via Functionally Pooled Stochastic Models," *Vertical Flight Society 77th Annual Forum, Online (due to COVID-19)*, AHS, 2021.

[39] Peters, D., and He, C., "A Finite-State Induced Flow Model for Rotors in Hover and Forward Flight," *American Helicopter Society 43rd Annual Forum, St. Louis, MO*, AHS, 1987.

[40] McKay, M., Niemiec, R., and Gandhi, F., "Post-Rotor-Failure-Performance of a Feedback Controller for a Hexacopter," *American Helicopter Society 74th Annual Forum, Phoenix, AZ*, AHS, 2018.

[41] Hakim, T. M. I., and Arifianto, O., "Implementation of Dryden Continuous Turbulence Model into Simulink for LSA-02 Flight Test Simulation," *Journal of Physics: Conference Series 1005(2018) 012017*, 2018.

[42] Davoudi, B., Taheri, E., Duraisamy, K., Jayaraman, B., and Kolmanovsky, I., "Quad-Rotor Flight Simulation in Realistic Atmospheric Conditions," *AIAA Journal*, Vol. 58, No. 5, 2020, pp. 1992–2004. https://doi.org/10.2514/1.J058327.

[43] Palomaki, R. T., Rose, N. T., van den Bossche, M., Sherman, T. J., and Wekker, S. F. J. D., "Wind Estimation in the Lower Atmosphere Using Multirotor Aircraft," *Journal of Atmospheric and Oceanic Technology*, 2017. https://doi.org/10.1175/JTECH-D-16-0177.1.

[44] Wang, B. H., Wang, D. B., Ali, Z. A., Ting, B. T., and Wang, H., "An Overview of Various Kinds of Wind Effects on Unmanned Aerial Vehicle," *Journal of Measurement and Control*, Vol. 52, No. 7-8, 2019, pp. 731–739. https://doi.org/10.1177/0020294019847688.

[45] Lan, H., "The Softmax Function, Neural Net Outputs as Probabilities, and Ensemble Classifiers," , November 2017. URL https://towardsdatascience.com/the-softmax-function-neural-net-outputs-as-probabilities-and-ensemble-classifiers-9bd94d75932, [Online; accessed 3-September-2020].